Article

Modelling Living Cells Response to Surface Tension and Chemical Patterns

Marco Macis, Francesca Lugli, and Francesco Zerbetto

Just Accepted

Modelling Living Cells Response to Surface Tension and Chemical Patterns

Marco Macis, Francesca Lugli, Francesco Zerbetto*

Dipartimento di Chimica "G. Ciamician", Università di Bologna, V. F. Selmi 2, 40126 Bologna, Italy

KEYWORDS Adherent cells, living cell shape, chemical patterns, surface tension, coarse-grained modelling

ABSTRACT Mechanobiology is an important epigenetic factor. It influences cell functioning and bears on gene induction, protein synthesis, cell growth and differentiation. In the presence of patterned chemical cues, living cells can take shapes that are far from that of a drop of fluid. These shapes are characterized by inward curvatures that are pinned at the points of location of the cues. The mechano-chemical interactions that orchestrate cell behavior is simulated and controlled by modeling the cells as made by parcels of fluid. Cells become drops that are then endowed with the presence of additional forces, generated on the fly, that effectively make them active. With the proper choice of the forces, the phenomena that emerge from the dynamics match quantitatively the experiments. A combination of hydrophilic and lipophilic forces acting between the beads of fluid allows the active drop to respond to patterned cues and form squares, pentagons, hexagons and flowers, just as living cells do.

Introduction

Living cells are highly complex systems characterized by a host of phenomena that continuously battle between equilibrium and non-equilibrium conditions. To provide a comprehensive understanding, their response to a variety of stimuli is constantly scrutinized both experimentally and computationally. Their geometrical structure and mechanical dynamics has far reaching consequences and governs their fate. Cells cultured on micropatterned substrates display different morphologies. Cell shape has been found to govern whether individual cells grow or die.[1] Living cells are viscoelastic. Upon expulsion from a micropipette, they take time to recover the original shape.[2] Satisfactory description of the process was obtained with very simple continuum modeling, which was based on a Newtonian fluid drop where the external membrane was represented by a layer characterized by a constant surface tension.[3] A more complex model consisted of the description of the cell with several regions characterized by different surface tensions and viscosities that represented the cytoplasm and the nucleus.[4] The cytoplasm was described either as a less viscous liquid or as a Maxwell fluid.[5] More recently, micro and nanostructural approaches were included in tensegrity models,[6] tense-cable models,[7] open-cell foam models,[8] and spectrin and actin networks.[9]

On the top of the response to micropipette aspiration, models have long been able to describe manipulation with optical tweezers and in laser traps,[10] magnetic twisting cytometry experiments,[11] AFM indentation,[12] and biomechanical properties obtained by a cytoindenter,[13] to name a few phenomena.

In cells and tissues, shape correlates with function. The behavior and fate of tissue cells are controlled by the rigidity and geometry of their adhesive environment, possibly through forces localized at the sites of adhesion. An important role in the shape/function connection is played by

the geometrical distribution of the tension. Bischofs et al. found that for cells whose sites of adhesion are restricted to small adhesive islands on a micropatterned substrate, the shape resembles a sequence of inward-curved circular arcs that look like epicycloids.[14] Quantitative image analysis revealed that the arc radii increase with the distance between the pinning points. Laplace law for interfaces under tension predicts circular arcs and does not explain the dependence on the spanning distance that was observed. Modeling, in conjunction with actomyosin inhibition experiments, suggested that cell shape is regulated by two different control modes related to motor contractility and structural changes in the actin cytoskeleton.

Banerjee and Giomi used a continuum model to investigate a living cell as a contractile film bound by an elastic cortex and connected to the substrate via elastic links.[15] When the adhesion sites were continuously distributed, the optimal cell shape was constrained by the adhesion geometry. For discrete adhesion sites, the cell shape was convex at weak contractility, while it developed local concavities at intermediate values of contractility. Increasing contractility beyond a critical value, the cell boundary underwent a discontinuous transition to a star-shaped configuration with cusps and protrusions, accompanied by the presence of a region of bistability and hysteresis.

Cells from different tissues respond to the stiffness and spatial patterning of their microenvironment by modulating shape and cortical stiffness. The interactions between substrate stiffness, cell shape, and cell stiffness were investigated using microfabricated arrays.[16] Cell cortical stiffness increased as a function of substrate stiffness and spread area. Soft substrates modulated cell cortical stiffness more than cell shape. An increase of the adherent area did not lead to cell stiffening. For cells constrained to a small area, cell shape effects are dominant over substrate stiffness and increasing substrate stiffness does not affect cell stiffness. Cell size and

substrate stiffness interact cooperatively or anticooperatively to enhance or antagonize each other.

Oakes et al. used fibroblasts to decouple the effects of substrate stiffness, focal adhesion density, and cell morphology.[17] By combining micropatterning with traction force microscopy experimental technique, they showed that the number of adhesion points and the substrate stiffness have little effect on the work done on the substrate by the cell. The local curvature along the cell edge governs the distribution and size of traction stresses to maintain constant strain energy.

Marchetti and coworkers used a continuum mechanical model to investigate an adherent cell on adhesive micropatterned substrates.[18] The cell was modeled as an isotropic and homogeneous elastic material subject to uniform internal contractile stresses. The build-up of tension from cortical actin bundles at the cell periphery was incorporated by an energy cost for bending the cell boundary, which effectively provided a resistance to changes in the local curvature. Integrin-based adhesions were modeled as harmonic springs that pin the cell to adhesive patches of a pre-defined geometry. They investigated the competing effects of bulk contractility and cortical bending rigidity in regulating cell shapes on non-adherent regions. They found that the crossover from convex to concave cell edges is controlled by the interplay between contractile stresses and boundary bending rigidity. In particular, the cell boundary became concave beyond a critical value of the contractile stress that was proportional to the cortical bending rigidity. The intracellular stresses were concentrated at the concave edge of the cell.

Bischofs et al. developed a continuum model of the cellular force distributions for cells adhering to adhesive patterns with different geometries and rigidities.[19] For adhesion along a continuous contour, forces are localized at the corners. For discrete sites of adhesion, the model

predicted that the forces are mainly determined by the lateral pull of the cell contour. Upon increasing the distance between two neighboring sites of adhesion, the adhesion force increases because the cell shape results in steeper pulling directions. Softer substrates generated smaller forces.

Kilian et al. demonstrated that cell shape has a strong influence on the differentiation of human mesenchymal stem cells, MSCs, from bone marrow.[20] Cells cultured in rectangles and pentagons displayed different adipogenesis and osteogenesis profiles. Geometric features that increase actomyosin contractility promote osteogenesis. Cytoskeletal-disrupting pharmacological agents modulated shape-based trends affecting focal adhesion and contractility during differentiation. Geometric shape cues can play a significant role in orchestrating the mechano-chemical signals and paracrine/autocrine factors that direct MSCs to appropriate fates.

The mechanical and physical behavior of a living cell depends on the complex and intertwined functioning of numerous subcellular components. In general, the main issue in developing continuum models for cell mechanics and physics is the choice of the proper differential law/equation able to capture the most important behavioral aspects of the cell under given experimental conditions. Crucial inputs for these models are the material constants/properties. Different types of experiments are described by different continuum models. It follows that it may be very hard to join or unify the different continuum descriptions. Nano- and micro-scale particle-based approaches, such as Monte Carlo and Molecular Dynamics simulations, are commonly used to study the mechanical characteristics and the structure of individual biomolecules, but cannot be used to simulate a cell as a whole. Mesoscopic coarse-grained methods have recently been used to investigate cell membranes,[21–24] cell tissues,[25] and blood hydrodynamics.[26]Recently, we proposed a particle-based model to simulate a variety of

properties of living cells.[27] Some morphological features and visco-elastic properties of drops - made by tens of thousands of beads- were matched to those of biological cells. The treatment described the interactions of the outer layer of cells with the surfaces of materials. An important feature of the model was that living cells appeared with their true size and the dynamics of the model is determined only by the forces between the constituent particles.

A crucial issue of the model was therefore how to describe the interactions between the "parcels of fluids", or beads, that made the cells. In analogy with other mesoscopic models,[21-26] the forces between the beads were described by very few quantities/parameters that could ideally be related to fundamental chemical forces such as hydro- and lipo-philicity. The values of such parameters represented an average of the properties of an area of the cells surface, or of a patch of material where the cell was attached.

The model was able to simulate the adhesion dynamics of living cells together with the motion of individual cells and the collective behavior of clusters of cells on materials. In silico, the drops were forced "to secrete" molecules. They became active soft matter objects that, differently from regular droplets, did not fuse when in contact. The cell trajectories were non-Brownian. The behavior that emerged from the simulations allowed ascribing some cell properties to their mechanics, rather than to their biochemical reactions and processes.

Here, we show how the proposed drop-like coarse-grained model is able to reproduce the process of cell adhesion onto chemically micropatterned surfaces. In particular, by explicitly simulating the dynamical process of adhesion formation, we were able to reproduce experimentally observed modifications of cell shapes modulated by different geometrical patterns.

The model

Differently from other particle-based method, in our model, the focus is not on the interaction energy but on the inter-particle forces. The simplest possible conservative interaction force between two mesoscopic particles is on/off or nearest neighbor. In order to generate particle dynamics/trajectories, that is changes of position in time, it is necessary to introduce the dependence of the force on the distance between the particles. A simple, perhaps the simplest, force dependence on the distance is linear and finite. It is a straight line that can be defined in a range between 0 and r_c, or in the range between $r_{c,1}$, $r_{c,2}$ as

$$\vec{F}_{ij}^c = \begin{cases} a_{ij}\left(1 - \frac{r_{ij}}{r_c}\right) \cdot \hat{n}_{ij}; & r_{ij} \leq r_c \\ 0 & ; \quad r_{ij} > r_c \end{cases} \tag{1a}$$

or

$$\vec{F}_{ij}^c = \begin{cases} b_{ij}\left(1 - \frac{r_{ij} - r_{c,1}}{r_{c,2} - r_{c,1}}\right) \cdot \hat{n}_{ij} & ; \quad r_{c,1} < r_{ij} < r_{c,2} \\ 0 & ; \quad r_{ij} < r_{c,1}; \ r_{ij} > r_{c,2} \end{cases} \tag{1b}$$

a_{ij} and b_{ij} are the strength of the force, which are set positive in Eq. (1a) and negative in Eq. (1b), $\hat{r}_{ij} = |\hat{r}_i - \hat{r}_j|$ is the inter-bead distance, r_c, $r_{c,1}$ and $r_{c,2}$ are cutoff, and $\hat{n}_{ij} = \frac{\hat{r}_{ij}}{|r_{ij}|}$ is a unit vector. The finite magnitude of the force makes the particles inter-penetrable as colloids. In polymers science, the polymer coarse-grained description at the Flory-Huggins level is based on positive values of a_{ij}. Notice that the use of a negative value for a_{ij} in Eq. (1a) would lead to particle fusion.

On the top of conservative forces, the dynamics is also governed by dissipative, $\hat{F}_{ij}^D$, and random forces, $\hat{F}_{ij}^R$. The balance between these forces controls the temperature.[28] A simple and effective choice is

$$\hat{F}_{ij}^{D} = -\gamma \omega^{D}(r_{ij})(\hat{n}_{ij} \cdot \hat{v}_{ij})\hat{n}_{ij} \tag{2}$$

and

$$\hat{F}_{ij}^{R} = \sigma \omega^{R}(r_{ij})\xi_{ij}\hat{n}_{ij}\delta t^{-1/2} \tag{3}$$

where, $\hat{v}_{ij} = \hat{v}_i - \hat{v}_j$ is the relative velocity of particles i and j, $\omega^{D}(r_{ij})$ and $\omega^{R}(r_{ij})$ are distance weighted functions for dissipative and random term, γ is the viscosity coefficient, σ is the noise strength, δt is the simulation time step, $\xi_{ij} = \xi_{ji}$ is a random variable, which cannot be velocity dependent if momentum must be conserved and usually follows Gaussian statistics with zero mean.[28,29] Notice that, this random variable, ξ_{ij}, may follow other distributions.[30] At equilibrium, dissipative and random forces cancel each other, and the dissipation fluctuation theorem holds if [31]

$$\omega^{D}(r_{ij}) = \left(\omega^{R}(r_{ij})\right)^2$$
$$\sigma^2 = 2\gamma k_B T/m \tag{4}$$

This set of conditions is called Dissipative Particle Dynamics, DPD,[28-31] and have found a large variety of applications in the investigation of materials and interfaces.[32-36]

The role of the balance between dissipative and random forces used here can be thought of as a clever thermostat that is obviously present when cells are functioning. The violation of the fluctuation-dissipation theorem observed in living cells is ascribed to non-equilibrium processes such as the generation of active forces.[37,38]
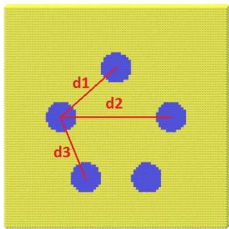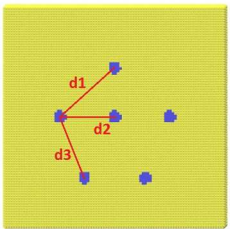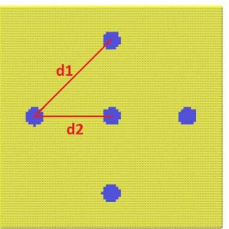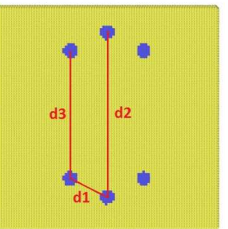
Details of the simulation

The simulations are run in dimensionless coordinates. The unit of length is set to r_c. For simplicity, $r_{c,1}$ is equal to r_c, while $r_{c,2}$ was set to 3.5 . The time step, δt, was set to 0.02 τ, where τ is the dimensionless time unit. The friction coefficient of the dissipative force, γ, was set to

5.61, the reduced temperature T^* was set to 0.53, a value representing a physical temperature T=310 K, as obtained through the relation T=133T^*+240.[23,39] Interestingly, for temperatures above 0.6, the cell integrity was not maintained.

The system consists of 220,000 beads distributed in a box 36×36×25 r_c. Periodic boundary conditions were used. The drop-like cell, C, was formed by about 10,350 beads, the surface, S, was 46,500 beads, and the medium, M, was 163,150 beads. The surface beads were arranged in five layers of a face-centered cubic structure that was frozen during the simulation. The density of the surface, ρ_S, was set to 15, a value higher than the rest of the fluids in the simulation box that was set to ρ_C=6 and ρ_M=6. The choice of ρ_S=15 was made to avoid the penetration of cell beads in the solid material.

Chemical adhesion patterns, P, on the surface were realized with different geometries following refs. (14) and (20), see also Table 1. During the simulations, part of the cell beads were converted into adhesion beads, A, mimicking the biological phenomenon of formation of cell-substrate adhesion complexes.

Table 1. Patterns features. Surface (S beads) in yellow, chemical adhesive pattern (P beads) in blue. Distances and radii in µm.

Features	Flower-like	Pentagon	Square	Stretched hexagon

Radius of each chemical cue	3.75	1.5	2.25	1.8
d_1	18.0	18.0	26.5	10.05
d_2	27.0	13.5	18.75	42.0
d_3	16.2	16.2		33.0
Total number of pattern beads of the cue spots	582	117	208	160

Based on the compressibility, Groot and Warren[40] identified for water at a density of 6 beads per point, a value of a_{ij} of 12.5, which therefore appears reasonable for a_{CC} and a_{MM}. The value of a_{CM}, set to 65, is rather phobic, but ensures that the cell in the medium preserves its integrity and mimics the presence of the membrane The interactions between cells and its adhesion regions and adhesion regions and the patterned regions are modeled with both repulsive (eq. 1a) and attractive (eq. 1b) forces. Table 2 lists all the parameter used in this work.

Table 2. List of all the a_{ij} and b_{ij} parameters (expressed in 10^{-11} N) used in this work.

	Cell	Adhesion	Medium	Surface	Pattern
Cell	$a_{CC} = 12.5$	$a_{CA} = 12.5$ $b_{CA} = -2.5$	$a_{CM} = 65$	$a_{CS} = 160$	$a_{CP} = 100$
Adhesion		$a_{AA} = 75$	$a_{AM} = 65$	$a_{AS} = 100$	$a_{AP} = 200$ $b_{AP} = -7.5$

Medium			$a_{MM} = 12.5$	$a_{MS} = 100$	$a_{MP} = 100$

At least five statistically independent simulations were carried out for each process of cell adhesion onto the different patterns in order to verify the robustness of the approach. A change of the initial random seed that starts each trajectory produces a different trajectory with identical model parameters. All the dynamics were performed with the same procedure that was divided into several steps:

1. After the design of the pattern on the surface, the cell beads are positioned above the surface as a spherical drop-like aggregate. No adhesion beads are present, the beads of the medium are placed outside the cell and fill the simulation box.

2. A minimum of 2,500 steps thermalize the system.

3. A list of C beads with a distance from P beads shorter than 3.5 r_c is generated and updated every 200 steps. At every step, a number of C particles in the list are transformed in A beads with a probability p

$$p = \left(1 - exp(-k\delta t)\right) \tag{5}$$

where k is empirically set to 0.05 and δt is the time step. For each C beads in the list, at every time step, a random number with a value between 0 and 1 is generated and compared with p. If the random number is smaller than p, the C particle is turned to A. The number of A beads that are created at every time step depends on the number of particles in the list, which, in turn, depends on how the cell covers the beads of the pattern.

In addition to the creation of A beads, a mechanism able to change A in C beads is introduced. When the distance from the surface becomes greater than 1.0 r_c, A are back-transformed into C

beads. This mechanism removes the excess of adhesion beads. It also helps in the dispersion of A beads on the P particles of the surface and obtains a more homogeneous and symmetric distribution of particles. The phase of creation and deletion of "adhesion particles" is performed for a total of at least 2,200 steps.

4. 2,500 more steps of equilibration are performed, during which no mechanism of beads transformation is active. At the end of this new equilibration, a final single conversion of A to C is executed to make sure that all A particles in excess are removed.

5. The total number of A beads is kept constant and only a few steps are necessary for re-equilibrating the system.

For each system, a reference run was performed where only soft repulsive interactions between A and P (a_{AP}= 200.0) and A and C (a_{AC}= 12.5) beads were applied.

All the calculations were carried out with the ESPResSO software.[41]

Mapping simulation parameters to physical values

The conversion of the dimensionless units of the simulation into physical parameters requires some assumptions and the use of experimental data. In practice, we assume the lengthscale of a bead and determine the timescale.

The lengthscale assumption is that 1 r_c = 1.5 μm, thus each bead has a radius of 0.51 μm. Such value is similar to that of organelles inside a living cell.[42,43] By setting 1 r_c = 1.5 μm, the cell diameter is 22.5 μm.

The diffusion coefficient of mitochondria in cytoplasm was found to be around 5×10^{-12} cm^2 s^{-1} (motion of mitochondria in cultured cells quantified by analysis of digitized images).[44] The calculation of the mean square displacement determines the self-diffusion coefficient of the

beads (D_{calc} = 0.016 r_c^2/τ), see Supporting Information. The time scale is determined by

comparing the calculated diffusion coefficient with that one of mitochondria, as

$$\tau = \frac{D^{calc}}{D^{exp}}[r_c]^2 = \frac{0.016}{5\times10^{-16}m^2/s} \times (1.5 \times 10^{-6}\ m)^2 \approx 70\ \text{s}. \tag{6}$$
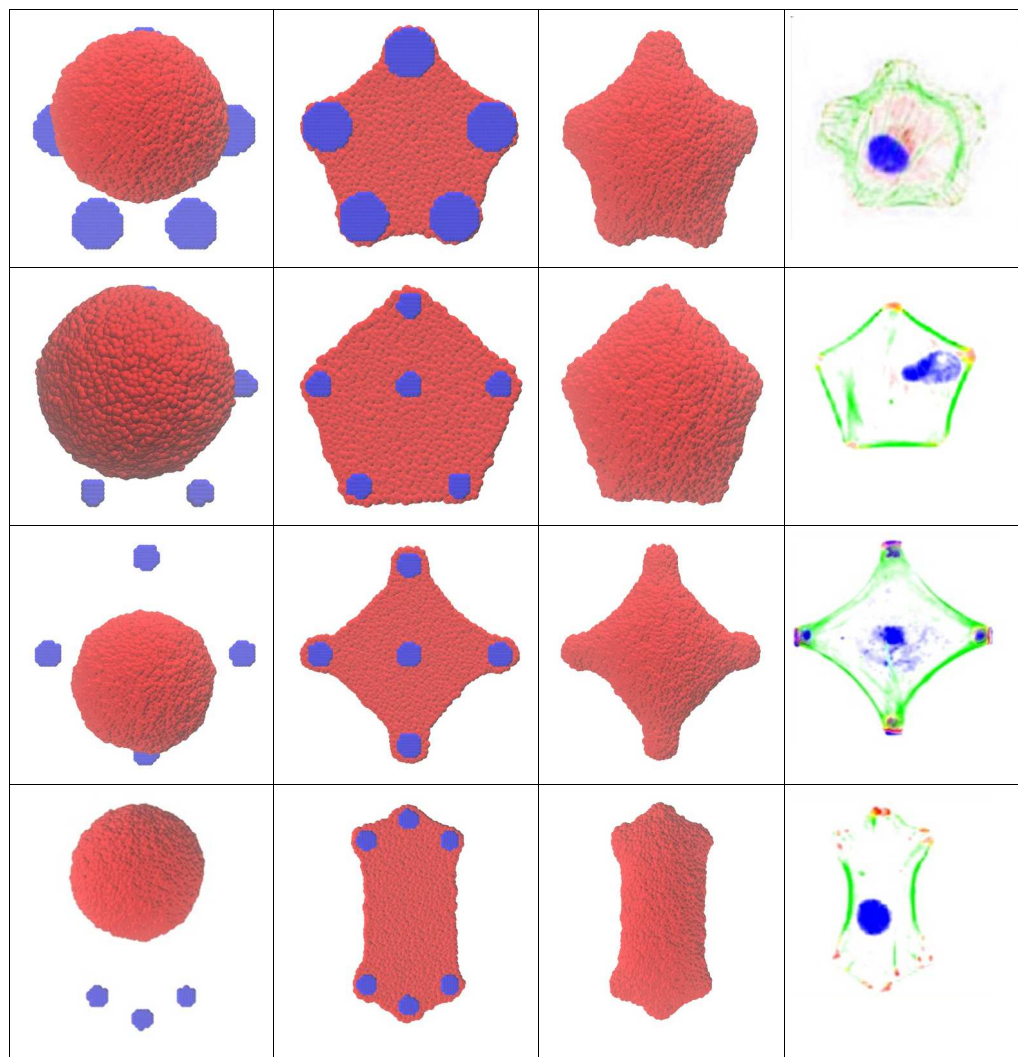
This timescale leads to an adhesion and deformation process that takes place in about 2 hours.

The timescale must be taken as only indicative, because of its dependence on the experimental

value of the diffusion coefficient. If we consider the diffusion coefficient of a spherical particle

of radius 0.5 μm, in a fluid with a viscosity comparable to that of the cytoplasm (70 cP), the

diffusion coefficient would be D = 0.65×10^{-14} m^2/s. With this value, the timescale becomes 6 sec,

which means that the adhesion process takes place in about 15 minutes. All results will be

presented in physical units.

Results and discussion

Four geometric cue patterns were investigated in the simulations. They are flower-like,

pentagon-like, square-like and stretched hexagon. Their interactions with living cells have been

reported experimentally.[14,20] The radius of the spot of the cues ranged from a minimum of 1.5

μm in the case of the pentagon pattern to a maximum of 3.75 μm for the flower arrangement.

The distances between the adhesion spots also varied over a factor of ~4, see Table 1. The

variation of the geometrical parameters introduces a variability of conditions that the "active

drop" has to cope with while adapting to the cues pattern.

For each geometrical arrangement, we performed a reference simulation (column 1 of Figure

1) where adhesion beads are generated (see Details of the simulations) without the presence of

any attractive force in the "active drop" (eq. 1a). These simulations show that drop/cell moves on

the pattern cues because of the favorable interactions but the cell/drop shape remains

substantially circular, as at the beginning of the simulations. This result shows that the drops to

spread on the surface cannot assume the geometries of the patterns without an additional

interaction.

Figure 1.Top to bottom: flower-like, pentagon-like, square-like and stretched hexagon patterns

that govern cell shape. Left to right: thermalized cell structure in the absence of A beads, A and

C beads adherent to the pattern, thermalized cell structure in the presence of A beads,

experimental cell shapes flower-like,[20] pentagon-like,[20] square-like,[14] stretched hexagon.[20]

As discussed in our previous work,[21] models based on fluid droplets can account for some features of living cells, mainly their passive response. In order to capture the active behavior of adhesive biological cells, we explicitly introduce in the coarse-grained cell/drop model the attractive interactions of eq. 1b. These forces are between A beads (which are generated on the fly inside the cell during the simulations) and the P beads located on the surface that represent the pattern of chemical cues. The dynamical simulations show that the spherical cell/drop, initially positioned on the surface, attaches and spreads on the cue spots. It modifies its shape (see columns 2 and 3 of Figure 1) in accordance with experimental observations (column 4 of Figure 1).

Cell adhesion dynamics

When biological cells in suspension contact a matrix-coated surface, they rapidly adhere and spread. In the "spread state", cells exert forces induced by actin polymerization and myosin contraction on the substrate through the generation of adhesion sites. As a consequence the cells initially flatten and deform extensively, increasing the contact area with the substrate. Figure 2 displays the spreading curves in time on the four different patterns.
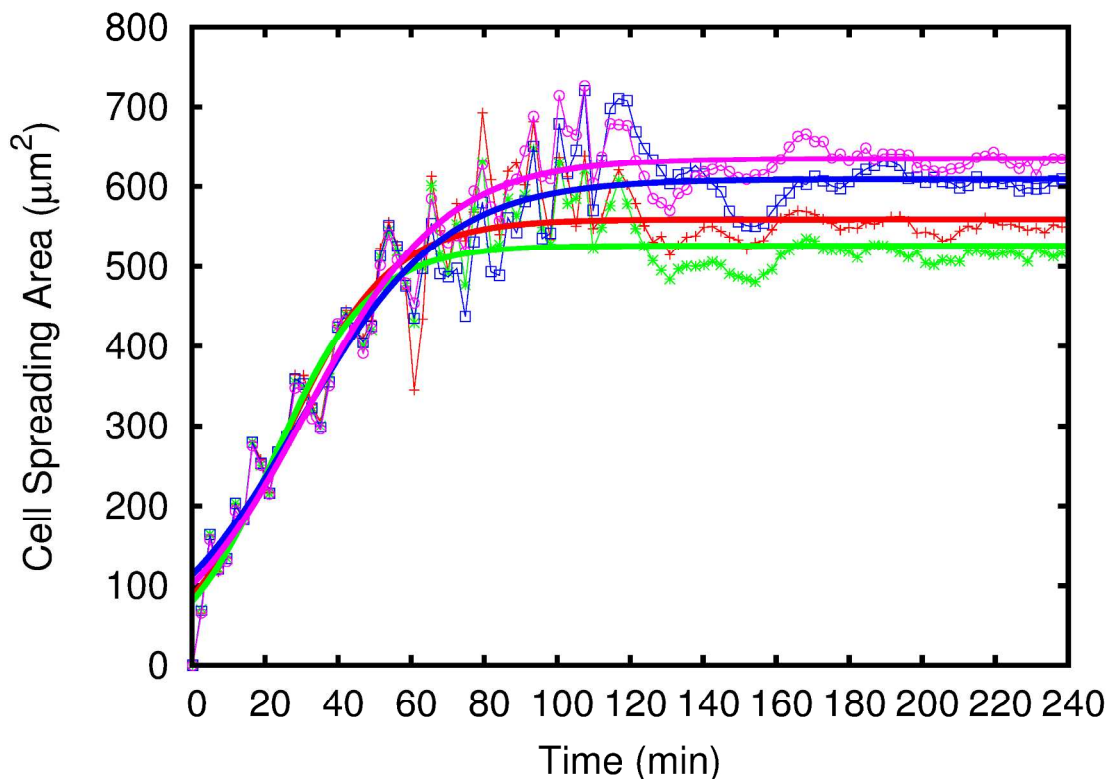
Figure 2. Spreading curves of the model cells on the four different patterns (red for flower-like, green for pentagon-like, blue for square-like and magenta for stretched hexagonal). The points correspond to simulation data averaged over five independent simulations (errors $\pm$ 5 μm^2). Solid lines correspond to fitted curve according to Eq. (8).

Spreading in all curves follows a sigmoidal evolution. Time t=0 corresponds to the instant when the spherical cell/drop contacts the surface, a "passive" spreading takes place, the cell increases its contact area because of favorable interactions between cell and surface beads, but the cell shape remains spherical. In the simulations, at t=60 min, the cell/drop starts expressing adhesion beads. Their number is proportional to the number of pattern beads. Adhesion beads anchor the cell to the substrate through attractive forces with the pattern beads and induce the cell/drop to further spread over the pattern, covering all the cue spots. Then, the cell contact area

reaches a plateau. The final cell-substrate contact area depends, not only on the number of pattern beads, but also on the geometry of the pattern.

It has been observed experimentally that the dynamics of biological cell spreading follows sigmoidal kinetics described by the logistic equation[45]

$$\frac{dA}{dt} = rA\left(1 - \frac{A}{A_{max}}\right) \tag{7}$$

where A_{max} is the maximum possible contact area of the cell and r is the rate constant of spreading.

The solution of this differential equation is

$$A(t) = \frac{A_{max}}{1 + \exp[-r(t-m)]} \tag{8}$$

where m, the constant of integration, gives the time at which the point of inflection occurs and the spreading area is equal to $A_{max}/2$. Fitting Eq. (8) to the data obtained from simulation yields the results given in Table 3.

Table 3. Parameters fitting logistic equation (Eq. (8)) to the simulation data reported in Figure 2. The values are averaged over five statistically independent runs.

Pattern	A_{max} (μm^2)	r (min^{-1})	m (min)
Flower-like	559 ± 4	0.0684 ± 0.005	25 ± 1
Pentagon-like	526 ± 4	0.0752 ± 0.006	23 ± 1
Square-like	609 ± 4	0.0504 ± 0.003	29 ± 1
Stretched hexagon	635 ± 3	0.0531 ± 0.002	31 ± 1

Recent experiments of spreading kinetics performed with highly adherent human cervical tumor cells (HeLa) on different values of density of integrin ligand RGD-motifs showed that while A_{max} is almost linearly dependent on the surface density of integrin ligands, the spreading parameter r is nearly constant and most likely depends on actin polymerization.[46]

Here we observe that the final contact area depends on the geometry of the pattern (the cell on the stretched hexagonal pattern has the greater A_{max}), and for similar geometry it weakly depends on the density of cue spot on the surface (the cell area on the flower-like pattern is slightly greater than the area on the pentagon-like).

For the four different geometries, the cell reaches the inflection point in about 30 min. These values are comparable with experimental parameters found for stem cells adhesion during differentiation.[47] The position of the inflection point actually is not affected by the attractive component of the forces exerted by the adhesion beads onto the surface. Experiments of spreading dynamics using reflection interference contrast microscopy carried out on different cell lines and substrate types suggested that cell spreading can be divided into two distinct stages: the earliest events that are characterized by passive adhesion and isotropic cell deformations, similar to the spreading of a liquid droplet on a surface, while the later stages involve the active mechanism of force generation by actin polymerization and myosin contraction.[48] The small differences in growth velocities are due to the different response of the cell/drop system to the creation of adhesion beads that can differ strongly in number in relation to the type of pattern. In general, the number of adhesion beads "expressed" by the cell/drop during the adhesion to the patterned surface is proportional to the amount of chemical cues (see Table 4).

Force exerted by the adhesion beads

The process of cell adhesion to an external substrate is mediated by cell-matrix adhesion complexes (CMAC). The complexes are specialized adhesive structures containing integrins and other adaptor proteins. They bind the cell to the extracellular matrix through the actin cytoskeleton. A variety of adhesion types exist, such as nascent adhesion, focal adhesion (growing and mature), fibrillar adhesion, stress fiber, and podosomes/invadopodia. The cell responds by eventually attaching to the substrate, exerting forces and modifying its shape.[49] Application of local external forces to cells was shown to stimulate the growth of size and force of adhesion sites, thus suggesting the mechanosensing behavior of focal adhesions.[50] In our model, adhesion beads (A) are generated dynamically on-the-fly during the simulation, starting at time t=60 min. A beads can be created only close to the chemical cue regions, and upon creation, they establish attractive forces with the pattern. This means that only if the cell senses the chemical pattern can produce adhesion sites. As the number of A beads increases, also the area of adhesion sites and the total exerted force increase. We have evaluated the mean force exercised by the A beads of the cell/drop on the surface. Our results are in good agreement with those presented by Balaban et. al.,[51] where the force applied by focal adhesion sites was measured for different types of cells, and are consistent with other estimations,[52,53] Table 4. The experiments performed on stationary adhesive cells showed that the stress measured at the different focal adhesions is constant at 5.5 ± 2 nN μm^{-2}. This value is comparable with the data obtained by simulations, where force/pattern surface ranges between 1.7 and 5.2 nN μm^{-2}.

Table 4. Force exerted by the adhesion beads, A, on the surface. Column 2: force expressed by a single A bead in the four different geometries; Columns 4 and 5: total force of A beads

normalized by the surface of the chemical pattern and the surface covered by the entire cell, respectively. The values are averaged over five statistically independent runs.

Geometry	Number of A beads	Force per A bead $(10^{-11}$ N)	Surface covered by the A beads (μm^2)	Force/Surface covered by the A beads $(nN/\mu m^2)$	Force/Surface covered by the cell/drop $(nN/\mu m^2)$
Flower-like	649 ± 8	-177.7 ± 0.8	220.9	5.22 ± 0.09	2.1 ± 0.1
Pentagon-like	137 ± 5	-53.1 ± 0.6	42.4	1.71 ± 0.08	0.1 ± 0.1
Square-like	416 ± 8	-66.1 ± 0.3	79.5	3.46 ± 0.08	0.5 ± 0.1
Stretched hexagon	254 ± 7	-65.2 ± 0.9	61.1	2.71 ± 0.1	0.3 ± 0.1

Characterization of the cell shape

Cells whose sites of adhesion are restricted to small adhesive islands on a micropatterned substrate present a sequence of inward-curved circular arcs.[14] These arcs appear spontaneously in the simulations. Figure 3 and Table 5 detail the concave curvatures on the four different patterns.
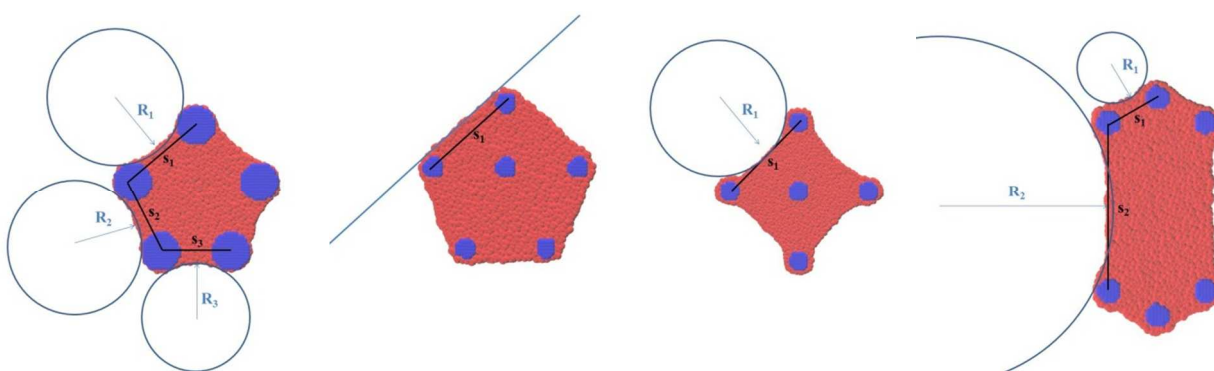

Figure 3. Fitted circular arcs to cell contours for the four patterns, from left to right, flower-like, pentagon-like, square-like and stretched hexagon.

Table 5. Curvatures of the cells/drops on the four patterns. *R* is the fitted arc radius and *s* is the distance between the cue spots. The values are averaged over five statistically independent runs.

	Flower-like		Pentagon-like		Square-like		Stretched Hexagon	
	s	R	s	R	s	R	s	R
1	18	15.7 ± 0.7	18	inf	26.5	22.6 ± 1.2	10.05	10.9 ± 0.4
2	16.2	14.3 ± 1.6					33.0	48.5 ± 3.1
3	9.4	12.7 ± 0.5						

In general, we observe that the curvature radius increases with the increase of the inter-cue distance, in agreement with experimental observations.[14] The curvature depends also on the dimension of the spot. The total area covered by cue spots for the flower-like pattern is ~5 times greater than the pentagon-like one. The number of adhesion beads generated in the pentagon is smaller and thus also the adhesion force. This geometry induces the cell/drop to spread homogeneously, without forming inward curves. In order to further investigate the effect of the pattern island size on the formation of inward curved circular arcs, we performed an additional simulation of cell adhesion on a pentagon-like pattern with a cue spot radius of 2.25 /μm. The variation of the pattern increases the force stress generated by the adhesion beads to 4.2 ± 0.1 nN/μm^2 with respect to the previous value of 1.71 ± 0.08 nN/μm^2. The results are in accordance with continuum models.[18, 19]

Cell-surface interfacial tension

It has been suggested that, similarly to liquid droplets whose shape is governed by the surface tension, also adhesive cells obey Laplace law where the mean radius of curvature R=2γ/p, with *γ*

the surface tension and p the pressure difference across the fluid interface.[14] Molecular dynamics

simulations can determine the interfacial tension as a function of the contact angle of the fluid on

a surface.[54,55] In practice, the cell/drop-surface interfacial tension γ_{MS} can be calculated with the

Young equation, as[56]

$$\gamma_{CS} = \gamma_{MS} - \gamma_{CM} cos\theta_C \tag{8}$$

where θ_C is the cell-surface contact angle and γ_{MS} and γ_{CM} are the medium–surface and cell–

medium interfacial tensions. Using Irving-Kirkwood equation,[57] which uses the three diagonal

components of the pressure tensor (see details in Supporting Information), we were able to

estimate the interfacial tension for medium-surface and cell-medium, which yields γ_{MS}= 0.233

mN/m and γ_{CM} = 0.251 mN/m. The cell/drop-surface tension (see Table 6) depends on the cell

contact angle, whose value is not constant along the perimeter of the cell. For this reason, the cell

contact angle was evaluated at two different points.

Table 6. Contact angle θ_C and interfacial tension γ_{CS} for the four different patterns used in the

simulations. For each geometry, we measured the contact angle at two different positions of the

cell/drop: the first value corresponds to the cell/drop contact angle in correspondence of the

tangential point of the circular arc, the second value is measured in correspondence of the

chemical cue. The values are averaged over five statistically independent runs.

Geometry	Contact angle θ_C (degree)	Interfacial tension γ_{CS} (mN/m)
Flower-like	75 ± 1	0.17 ± 0.02
	49 ± 2	0.07 ± 0.02
Pentagon-like	79 ± 1	0.18 ± 0.02

	48 ± 3	0.06 ± 0.04
Square-like	84 ± 1	0.21 ± 0.02
	42 ± 2	0.05 ± 0.02
Stretched	81 ± 2	0.19 ± 0.02
	42 ± 0.4	0.05 ± 0.01

Measurement of two contact angles for each shape shows the effect of the position of the chemical spots and the adhesion sites. A beads interact only with the area of the cell around adhesion sites (small contact angles) and do not affect cell adhesion in the remaining parts (large contact angles). Reference simulations with cells/drops characterized by quasi-circular shapes found contact angle values of ~85°. These contact angle values are comparable with experimental contact angles measured with lateral microscopy techniques for different cell lines on different surfaces.[58] During the active adhesion phase, the cells lower their interfacial tension with a surface (initial surface tension = 0.211 nN/m), in particular in areas where adhesion beads are concentrated. The process allows the cell/drops to spread on the surface and increase, not only its contact with the surface, but also the area of the cell/drops exposed to the medium. Since the surface tension relates to the work required to extend a surface of a fluid in contact with another fluid, the process of adhesion beads creation that takes place in the simulations, in combination with the attractive force applied, is equivalent to supply energy to win the cell-medium surface tension.

Conclusion

In this work, a coarse-grained model to describe living cells was developed to simulate the process of cell adhesion onto chemically patterned surfaces. During the simulations, adhesion beads are dynamically generated inside the cell in proximity of the chemical cues. The adhesion beads pin the cell to the patterned surface. The expression of adhesion beads (whose rate was properly tuned) leads to an adhesion process whose spreading kinetics follows a logistic function. The parameters of the logistic equation are comparable with those found experimentally.[47] The forces generated in the dynamics reproduce the experimental focal adhesion stress of 5.5 ± 2 nN μm^{-2}.[50]

Living cells attached to surfaces, characterized by the presence of small adhesive spots, take shapes with inward-curved circular arcs. The radius of curvature of these arcs depends on the distances between the spots of the pattern and on the size of the spots. The simulations spontaneously reproduce the living cell behavior. In practice, the process of adhesion bead generation inside the cell correctly mimics the energy use of the cell to adhere to complicated surfaces.

Ideally, our approach allows to treat different cell properties such as morphology, spreading kinetics and motility under different conditions in a unified manner. The parameters used in this work are generic and are not ascribable to any particular cell line or cell/surface interaction. In the future, they may be specialized to cell lines or materials. The main limitation of the model arises from the spatial resolution of the beads, each one of which representing a portion of cell of micrometer size. Increasing the resolution is possible, but implies an increase of computational cost.

Understanding mechanical cellular processes can assist in the optimization of biomimetic materials and in the control of the cell response to the presence of new environments.

1
2
3
4
5
6
7
8
9
10
11
12
13
14
15
16
17
18
19
20
21
22
23
24
25
26
27
28
29
30
31
32
33
34
35
36
37
38
39
40
41
42
43
44
45
46
47
48
49
50
51
52
53
54
55
56
57
58
59
60

ASSOCIATED CONTENT

Supporting Information. Calculation of the cell beads diffusion coefficient; Curvatures of the cell on the pentagon-like pattern as a function of the cue spot size; computational details of the cell-surface interfacial tension calculation. (PDF) Four movies of the dynamics of cell adhesion onto the different patterns (flower.gif, pentagon.gif, square.gif, stretched.gif). (GIF)

AUTHOR INFORMATION

Corresponding Author

*E-mail: francesco.zerbetto@unibo.it. Phone: +39 051 2099473

Author Contributions

The work was carried and the manuscript was written with contributions of all authors. All authors have given approval to the final version of the manuscript.

REFERENCES

1. Chen, C. S.; Mrksich, M.; Huang, S.; Whitesides, G. M.; Ingber, D. E. Geometric Control of Cell Life and Death. *Science* **1997**, *276*, 1425-1428.

2. Lim, C.T.; Zhou, E.H.; Quek, S.T. Mechanical Models for Living Cells—a Review. *J. Biomechanics* **2006**, *39*, 195–216.

3. Yeung, A., Evans, E. Cortical Shell–Liquid Core Model for Passive Flow of Liquid-Like Spherical Cells into Micropipets. *Biophys. J.* **1989**, *56*, 139–149.

4. Kan, H.C.; Udaykumar, H.S.; Shyy, W.; Tran-Son-Tay, R. Hydrodynamics of a Compound Drop with Application to Leukocyte Modeling. *Physics of Fluids* **1998**, *10*, 760–774.

5. Dong, C.; Skalak, R.; Sung, K.L.; Schmid-Schonbein, G.W.; Chien, S. Passive Deformation Analysis of Human Leukocytes. *J. Biomech. Engin.* **1988**, *110*, 27–36.

6. Stamenovic, D.; Fredberg, J.J.; Wang, N.; Butler, J.P.; Ingber, D.E. A Microstructural Approach to Cytoskeletal Mechanics Based on Tensegrity. *J. Theor. Biol.* **1996**, *181*, 125–136.

7. Coughlin, M.F.; Stamenovic, D. A Prestressed Cable Network Model of the Adherent Cell Cytoskeleton. *Biophys. J.* **2003**, *84*, 1328–1336.

8. Satcher Jr. R.L.; Dewey Jr., C.F. Theoretical Estimates of Mechanical Properties of the Endothelial Cell Cytoskeleton. *Biophys. J.* **1996**, *71*, 109–118.

9. Kim, T.; Hwang, W.; Lee, H.; Kamm R.D. Computational Analysis of Viscoelastic Properties of Crosslinked Actin Networks. *PLoS Comp. Biol.* **2009**, *5*, e1000439.

10. Henon, S.; Lenormand, G.; Richert, A.; Gallet, F. A New Determination of the Shear Modulus of the Human Erythrocyte Membrane Using Optical Tweezers. *Biophys. J.* **1999**, *76*, 1145–1151.

11. Wang, N.; Butler, J.P.; Ingber, D.E.. Mechanotransduction Across the Cell Surface and Through the Cytoskeleton. *Science* **1993**, *260*, 1124–1127.

12. Hoh, J.H.; Schoenenberger, C.A.. Surface Morphology and Mechanical Properties of MDCK Monolayers by Atomic Force Microscopy. *J. Cell Sci.* **1994**, *107*, 1105–1114.

13. Shin, D.; Athanasiou, K. Cytoindentation for Obtaining Cell Biomechanical Properties. *J. Orthop. Res.* **1999**, *17*, 880–890.

14. Bischofs, I.B.; Klein, F.; Lehnert, D.; Bastmeyer, M.; Schwarz, U.S. Filamentous Network Mechanics and Active Contractility Determine Cell and Tissue Shape. *Bioph. J.* **2008**, *95*, 3488–3496.

15. Banerjee, S.; Giomi, L. Polymorphism and Bistability in Adherent Cells. *Soft Matter* **2013**, *9*, 5251- 5260.

16. Tee, S.-Y.; Fu, J.; Chen, C. S.; Janmey, P. A. Cell Shape and Substrate Rigidity Both Regulate Cell Stiffness. *Biophys. J.* **2011**, *100*, L25–L27.

17. Oakes, P. W.; Banerjee, S.; Marchetti, M. C.; Gardel, M.L. Geometry Regulates Traction Stresses in Adherent Cells. *Biophys J.* **2014**, *1074*, 825–833.

18. Banerjee, S.; Sknepnek, R.; Marchetti, M.C. Optimal Shapes and Stresses of Adherent Cells on Patterned Substrates. *Soft Matter*, **2014**, *10*, 2424-2430.

19. Bischofs, I. B.; Schmidt, S. S.; Schwarz, U. S. Effect of Adhesion Geometry and Rigidity on Cellular Force Distributions. *Phys. Rev. Lett.* **2009**, *103*, 048101.

20. Kilian, K.A.; Bugarij, B.; Lahn, B. T.; Mrksich M. Geometric Cues for Directing the Differentiation of Mesenchymal Stem Cells. *Proc. Natl. Acad. Sci. USA* **2010**, *107*, 4872–4877.

21. Shillcock, J.; Lipowsky, R. Tension-Induced Fusion of Bilayer Membranes and Vesicles. *Nat. Mater.* **2005**, *4*, 225-228.

22. Groot, R. D.; Rabone, K. L. Mesoscopic Simulation of Cell Membrane Damage, Morphology Change and Rupture by Nonionic Surfactants. *Biophys. J.* **2001**, 81, 725-736.

23. M. Venturoli, B. Smit and M. M. Sperotto, Simulation Studies of Protein-Induced Bilayer Deformations, and Lipid-Induced Protein Tilting, on a Mesoscopic Model for Lipid Bilayers with Embedded Proteins. *Biophys. J.* **2005**, *88*, 1778-1798.

24. Reynwar, B. J.; Illya, G.; Harmandaris, V. A.; Müller, M. M.; Kremer, K., Deserno, M. Aggregation and Vesiculation of Membrane Proteins by Curvature-Mediated Interactions. *Nature* **2007**, *447*, 461-464.

25. Basan, M.; Prost, J.; Joanny, J. F.; Elgeti, Dissipative Particle Dynamics Simulations for Biological Tissues: Rheology and Competition. *J. Phys. Biol.* **2011**, *8*, 026014.

26. Fedosov, D. A.; Caswell, B.; Karniadakis, G. E. A Multiscale Red Blood Cell Model with Accurate Mechanics, Rheology, and Dynamics. *Biophys. J.* **2010**, *98*, 2215-2225.

27. Dallavalle, M.; Lugli, F.; Rapino, S.; Zerbetto, F. "Active" Drops as Phantom Models for Living Cells. A mesoscopic Particle-Based Approach. *Soft Matter*, **2016**, *12*, 3538-3544.

28. Hoogerbrugge, P. J.; Koelman, J. M. V. A. Simulating Microscopic Hydrodynamic Phenomena with Dissipative Particle Dynamics. *Europhys. Lett.* **1992**, *19*, 155-160.

29. Koelman, J. M. V. A.; Hoogerbrugge, P. J. Dynamic Simulations of Hard-Sphere Suspensions Under Steady Shear. *Europhys. Lett.* **1993**, *21*, 363-368.

30. Nikunen, P.; Karttunen, M.; Vattulainen, I. How Would You Integrate the Equations of Motion in Dissipative Particle Dynamics Simulations? *Comput. Phys. Commun.* **2003**, *153*, 407-423.

31. Espanol, P.; Warren, P. Statistical Mechanics of Dissipative Particles Dynamics. *Europhys. Lett.* **1995**, *30*, 191-196.

32. Liu, Y; Kuksenok, O; He, XM.; Aizenberg, M.; Aizenberg, J.; Balazs, A.C.; Liu, Y.; Harnessing Cooperative Interactions between Thermoresponsive Aptamers and Gels To Trap and Release Nanoparticles, *ACS appl. mater. & interf.*, **2016**, *8*, 30475-30483

33. Ge, W.Y.; Li, N.K.; McCormick, R.D.; Lichtenberg, E.; Yingling, Y.G.; Stiff-Roberts, A.D.; Emulsion-Based RIR-MAPLE Deposition of Conjugated Polymers: Primary Solvent Effect and Its Implications on Organic Solar Cell Performance, *ACS appl. mater. & interf.* **2016**, *8*, 19494-19506

34. Wang, Y; Li, Q.Y.; Liu, X.B.; Zhang, C.Y.; Wu, Z.M.; Guo, X.D., Mesoscale Simulations and Experimental Studies of pH-Sensitive Micelles for Controlled Drug Delivery *ACS appl. mater. & interf.* **2015**, *7*, 25592-25600.

35. Leonforte, F.; Muller, M.; Poly(N-isopropylacrylamide)-Based Mixed Brushes: A Computer Simulation Study, *ACS appl. mater. & interf.* **2015**, *7*, 12450-12462,

36. Dallavalle, M.; Calvaresi, M.; Bottoni, A.; Melle-Franco, M.; Zerbetto, F. Graphene Can Wreak Havoc with Cell Membranes *ACS appl. mater. & interf.* **2015**, *7*, 4406-4414.

37. Mizuno, D.; Tardin, C.; Schmidt, C. F.; MacKintosh, F. C. Nonequilibrium Mechanics of Active Cytoskeletal Networks. *Science* **2007**, *315*, 370-373.

38. Turlier, H.; Fedosov, D. A.; Audoly, B.; Auth, T.; Gov, N. S.; Sykes, C.; Joanny, J.-F.; Gompper, G.; Betz, T. Equilibrium Physics Breakdown Reveals the Active Nature of Red Blood Cell Flickering. *Nat. Phys.* **2016**, *12*, 513–519.

39. Li, X.; Pivkin, I. V.; Liang, H.; Karniadakis, G. E. Shape Transformations of Membrane Vesicles from Amphiphilic Triblock Copolymers: a Dissipative Particle Dynamics Simulation Study. *Macromolecules* **2009**, *42*, 3195- 3200.

40. Groot, R. D.; Warren, P. B. Dissipative Particle Dynamics: Bridging the Gap between Atomistic and Mesoscopic Simulation. *J. Chem. Phys.* **1997**,*107*, 4423-4435.

41. Limbach, H. J.; Arnold, A.; Mann, B. A.; Holm, C. ESPResSo—an Extensible Simulation Package for Research on Soft Matter Systems. *Comput. Phys. Commun.* **2006**, *174*, 704-727.

42. Kuehnel, W. Color Atlas of Cytology, Histology, & Microscopic Anatomy, 4th edition; Thieme: Stuttgart, 2003.

43. Wiemerslage, L.; Lee, D. Quantification of Mitochondrial Morphology in Neurites of Dopaminergic Neurons using Multiple Parameters. *J Neurosci Methods* **2016**, *262*, 56-65.

44. Salmeen, I.; Zacmanidis, P.; Jesion, G.; Feldkamp, L.A. Motion of Mitochondria in Cultured Cells Quantified by Analysis of Digitized Images. *Biophys. J.* **1985**, *48*, 681-686.

45. Bardsley, W. G.; Aplin, J. D. Kinetic Analysis of Cell Spreading. I. Theory and Modeling of Curves. *J. Cell Sci.*, **1983**, *61*, 365-373.

46. Orgovan, N.; Peter, B.; Bosze, S.; Ramsden, J. J.; Szabo, B.; Horvarth, R. Dependence of Cancer Cell Adhesion Kinetics on Integrin Ligand Surface Density Measured by a High-Throughput Label-Free Resonant Waveguide Grating Biosensor. *Sci. Rep.* **2014**, *4*, 4034.

47. Aref, A.; Horvath, R.; Ramsden, J. J. Spreading Kinetics for Quantifying Cell State During Stem Cell Differentiation. *J. Biol. Phys. Chem.* **2010**, *10*, 145-151.

48. Cuvelier, D.; Théry, M.; Chu, Y.-S.; Dufour, S.; Thiéry, J.-P.; Bornens, M.; Nassoy, P.; Mahadevan, L. The Universal Dynamics of Cell Spreading. *Curr. Biol.* **2007**, *17*, 694-699.

49. Geiger, B.; Spatz, J. P.; Bershadsky, A. D. Environmental Sensing Through Focal Adhesion. *Nat. Rev. Mol. Cell Bio.* **2009**, *10*, 21-33.

50. Riveline, D.; Zamir, E.; Balaban, N. Q.; Schwarz, U. S.; Ishizaki, T.; Narumiya, S.; Kam, Z.; Geiger, B.; Bershadsky, A. D. Focal Contacts as Mechanosensors: Externally Applied Local Mechanical Force Induces Growth of Focal Contacts by an mDia1-Dependent and ROCK-Independent Mechanism. *J Cell Biol* **2001**, *153*, 1175-1186.

51. Balaban, N. Q.; Schwarz, U. S.; Riveline, D.; Goichberg, P.; Tzur, G.; Sabanay, I.; Mahalu, D.; Safran, S.; Bershadsky, A.; Addadi, L.; Geiger, B. Force and Focal Adhesion Assembly: a Close Relationship Studied Using Elastic Micropatterned Substrates. *Nat Cell Biol* **2001**, *3*, 466-472.

52. Galbraith, C. G.; Sheetz, M. P. A Micromachined Device Provides a New Bend on Fibroblast Traction Forces. *Proc. Natl Acad. Sci. USA* **1997**, *94*, 9114-9118.

53. Dembo, M.; Wang, Y. L. Stresses at the Cell-to-Substrate Interface During Locomotion of Fibroblasts. *Biophys J.* **1999**, *76*, 2307-2316.

54. Jones, J. L.; Lal, M.; Ruddock, J. N.; Spenley, N. A. Dynamics of a Drop at a Liquid-Solid Interface in Simple Shear Fields: A Mesoscopic Simulation Study. *Faraday Discuss.,* **1999**, *112*, 129-142.

55. Kong, B.; Yang, X. Dissipative Particle Dynamics Simulation of Contact Angle Hysteresis on a Patterned Solid/Air Composite Surface. *Langmuir* **2006**, *22*, 2065-2073.

56. Young, T. An Essay on the Cohesion of Fluids. *Philos. Trans. R. Soc. Lond.* **1805**, *95*, 65-87.

57. Irving, J. H.; Kirkwood, J. G. The Statistical Mechanical Theory of Transport Processes. IV. The Equations of Hydrodynamics. *J. Chem. Phys.* **1950**, *18*, 817-829.

58. Walz, J. A.; Lui, I.; Wilson, D. J.; Mace, C. R. Lateral Microscope Enables the Direct Observation of Cellular Interface and Quantification of Changes in Cell Morphology during Adhesion. *ACS Biomat. Sci. & Eng.* **2016**, *2*, 1367-1375.

TOC

1
2
3
4
5
6
7
8
9
10
11
12
13
14
15
16
17
18
19
20
21
22
23
24
25
26
27
28
29
30
31
32
33
34
35
36
37
38
39
40
41
42
43
44
45
46
47
48
49
50
51
52
53
54
55
56
57
58
59
60